Influence of the polarization in grazing scattering of fast helium atoms from LiF(001) surfaces

M. S. Gravielle and J. E. Miraglia
Instituto de Astronomía y Física del Espacio, CONICET, Casilla de Correo 67, Sucursal 28, 1428 Buenos Aires, Argentina and Departamento de Física, FCEN, Universidad de Buenos Aires, Buenos Aires, Argentina

(Received 13 May 2008; revised manuscript received 15 July 2008; published 26 August 2008)

Grazing scattering of neutral atoms from insulator surfaces is investigated in the intermediate velocity range, in which interference effects have recently been observed. To describe this process we introduce a distorted-wave method based on the use of the eikonal wave function, which takes into account the phase of the scattering state along the classical projectile path. The eikonal theory is applied to evaluate the angular distribution of few-keV helium atoms after impinging on a LiF(001) surface along low-index crystallographic directions. The interest focuses on the role played by the projectile polarization produced by cations and anions of the crystal surface. For the considered collision system we found a polarization channel, corresponding to the direction ⟨110⟩, which is affected by this effect, while for incidence in the direction ⟨100⟩ the polarization contribution is nearly negligible. The proposed eikonal approach, including polarization effects, provides angular projectile spectra in good agreement with the experimental data.

DOI: 10.1103/PhysRevA.78.022901 PACS number(s): 34.35.+a, 61.85.+p

I. INTRODUCTION

Experimental evidence of interference effects produced during grazing scattering of fast atoms from insulator surfaces were recently presented in Refs. [1–3]. Under axial surface channeling conditions, the reported measurements of scattered projectile distributions display well-defined spots, associated with diffraction patterns originated by the periodic structure of the crystal. Even though the diffraction of particles from crystal surfaces has been a well-understood phenomena from the beginning of quantum mechanics, the importance of these experimental results is due to the effect not being expected to be observable for light atoms with energies in the keV range, whose de Broglie wavelengths are some orders of magnitude smaller than the shortest interatomic distance in the crystal.

Two different interference mechanisms have been proposed to explain the experimental observations. The first of them [1,2] is related to the diffraction by a periodic lattice and relies on the assumption that the projectile motion perpendicular to the axial incidence channel can be decoupled from the parallel one. The semiclassical approach [2] proposed for the description of this mechanism predicts a maximum in the distribution when the component normal to the scattering plane of the final projectile momentum coincides with a reciprocal lattice vector. Such a result, also confirmed by means of a wave packet propagation approach [2], is in accord with the experimental data for the lowest impact energies [1,2]. The second mechanism [3], called a supernumerary rainbow, is originated by the corrugation of the surface potential, which gives rise to a quantum interference between projectiles emerging from the surface with the same direction but reflected at different turning points [4].

To describe the experimentally observed patterns, in this article we introduce a distorted-wave model, called the surface eikonal approximation, which is valid for small de Broglie wavelengths of incident atoms. This method makes use of the eikonal wave function [5] to represent the elastic collision with the surface, while the projectile movement is classically described, taking into account different initial conditions. The surface eikonal approach can be considered as an extension of the well-known Glauber approximation [6] for collisions with corrugated surfaces [7] instead of atoms, but considering axial channeled trajectories. It includes both interference mechanisms and the idea behind it essentially coincides with that of the semiclassical formalism [4] used in Ref. [3].

The surface eikonal approach is here employed to describe angular distributions of swift He^0 atoms scattered off from a LiF(001) surface, for which there are experimental data available [1–3]. As the considered process is very sensitive to the description of the surface potential, the aim of the work is to investigate the influence of the polarization on the interference patterns. In our model the interaction of the incident atom with the crystal surface is represented as a sum of individual interatomic potentials, which take into account the contribution of the different ionic centres of the insulator material [8]. To evaluate the interatomic potentials we use the Abrahamson approximation [9], adding the asymptotic contribution of the projectile polarization. The role of the polarization is analyzed for incidence along the ⟨100⟩ and ⟨100⟩ channels, finding that polarization effects are important for this latter crystallographic direction. Atomic units ($e^2 = \hbar = m_e = 1$) are used unless otherwise stated.

II. SURFACE EIKONAL APPROXIMATION

Let us consider the grazing impact of an atomic projectile (P), with mass m_P, on a crystal surface (S). As a result of the collision, the projectile with initial momentum $\vec{K}_i$ is elastically scattered from the surface, ending in a final state with momentum $\vec{K}_f$. The frame of reference is fixed on a target ion belonging to the first atomic layer, with the surface contained in the x-y plane and the $\hat{z}$ versor perpendicular to the surface, aiming towards the vacuum region.

We assume that the state Ψ_i^+ associated with the collision system satisfies the time-independent Schrödinger equation for the Hamiltonian

 ©2008 The American Physical Society

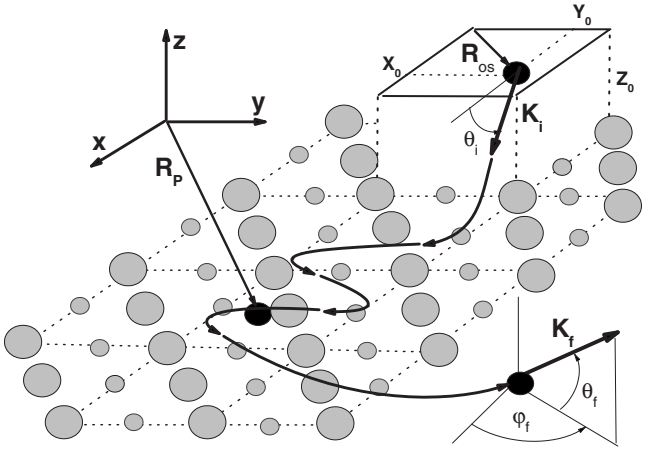

FIG. 1. Schematic depiction of the coordinate system.

$$H = -\frac{1}{2m_P}\nabla^2_{\vec{R}_P} + V_{\rm SP}(\vec{R}_P), \tag{1}$$

where $\vec{R}_P$ denotes the position of the center-of-mass of the incident atom and $V_{\rm SP}$ is the surface-projectile interaction. As initial condition, when the projectile is far from the surface, Ψ_i^+ tends to the state Φ_i, with $\Phi_j(\vec{R}_P)=(2\pi)^{-3/2}\exp(i\vec{K}_j\cdot\vec{R}_P)$, $j=i(f)$, the initial (final) unperturbed wave function.

The central magnitude to describe the elastic scattering process is the transition matrix, which reads

$$T_{if} = \int d\vec{R}_P \Phi_f^*(\vec{R}_P) V_{\rm SP}(\vec{R}_P)\Psi_i^+(\vec{R}_P). \tag{2}$$

In the energy range of interest, Eq. (2) can be expressed in terms of the classical trajectory of the projectile $\vec{\mathcal{R}}_P$ by means of the substitution $\vec{R}_P \cong \vec{\mathcal{R}}_P$, as in the usual semiclassical formalism [10]. The position $\vec{\mathcal{R}}_P$ of the incident atom at a given time t is governed by the Newton equations associated with the potential $V_{\rm SP}$, verifying the relation $\vec{\mathcal{R}}_P(\vec{R}_{os},t) = \vec{R}_{os} + Z_o\hat{z} + \int_{-\infty}^t dt'\vec{v}(\vec{R}_{os},t')$, where $\vec{v}(\vec{R}_{os},t)$ is the classical velocity of the projectile, $\vec{R}_{os}=(X_o,Y_o,0)$ identifies its initial position on the surface plane, and $Z_o \to +\infty$. A sketch picture of the projectile path and the coordinate system is displayed in Fig. 1. By replacing the integration variables $\vec{R}_P = (X_P,Y_P,Z_P)$ by the new ones $\{X_o,Y_o,t\}$ in Eq. (2), the transition matrix is expressed as [11]

$$T_{if} = \int d\vec{R}_{os}\int_{-\infty}^{+\infty} dt |v_z(\vec{R}_{os},t)| \Phi_f^*(\vec{\mathcal{R}}_P) V_{\rm SP}(\vec{\mathcal{R}}_P)\Psi_i^+(\vec{\mathcal{R}}_P), \tag{3}$$

where $v_z(\vec{R}_{os},t)$ is the component of $\vec{v}$ normal to the surface.

Since the de Broglie wavelength of the incident projectile $\lambda = 2\pi/K_i$ is sufficiently short compared with the characteristic distance of the surface potential, we approximate the scattering state Ψ_i^+ by means of the eikonal wave function [5], i.e.,

$$\Psi_i^+(\vec{\mathcal{R}}_P) \simeq \chi_i^{(eik)+}(\vec{\mathcal{R}}_P) = \Phi_i(\vec{\mathcal{R}}_P)\exp[-i\eta(\vec{\mathcal{R}}_P)], \tag{4}$$

where $\eta(\vec{\mathcal{R}}_P)$ is the eikonal phase, defined as

$$\eta(\vec{\mathcal{R}}_P(\vec{R}_{os},t)) = \int_{-\infty}^t dt' V_{\rm SP}(\vec{\mathcal{R}}_P(\vec{R}_{os},t')). \tag{5}$$

By introducing the function $\chi_i^{(eik)+}$ in Eq. (3) the eikonal transition matrix reads

$$T_{if}^{(eik)} = \frac{1}{(2\pi)^3}\int d\vec{R}_{os}\int_{-\infty}^{+\infty} dt |v_z(\vec{R}_{os},t)| \times \exp[-i\vec{Q}\cdot\vec{\mathcal{R}}_P - i\eta(\vec{\mathcal{R}}_P)]V_{\rm SP}(\vec{\mathcal{R}}_P), \tag{6}$$

where $\vec{Q}=\vec{K}_f-\vec{K}_i$ is the projectile momentum transfer and the final momentum $\vec{K}_f$ satisfies the energy conservation, i.e., $K_f=K_i$. The differential probability, per unit of surface area, of elastic scattering with final momentum $\vec{K}_f$ in the direction of the solid angle Ω_f is obtained from Eq. (6) as $dP/d\Omega_f = (2\pi)^4 m_P^2 |\tilde{T}_{if}^{(eik)}|^2$, where $\tilde{T}_{if}^{(eik)}$ denotes the eikonal T-matrix element, normalized per unit area. Note that the main difference between the usual eikonal scattering amplitude [5,7] and Eq. (6) arises from the use of axial channeled trajectories instead of straight-line ones.

The first-order-Born T-matrix element can be derived from Eq. (6) by neglecting the eikonal phase; that is, by fixing $\eta(\vec{\mathcal{R}}_P)=0$. It reads

$$T_{if}^{\rm Born} = \frac{1}{(2\pi)^3}\int d\vec{R}_{os}\int_{-\infty}^{+\infty} dt |v_z(\vec{R}_{os},t)| \times \exp(-i\vec{Q}\cdot\vec{\mathcal{R}}_P)V_{\rm SP}(\vec{\mathcal{R}}_P). \tag{7}$$

III. INTERACTION POTENTIALS

In this work, the projectile-surface potential $V_{\rm SP}$ contains the static and polarization interactions, i.e., $V_{\rm SP}=V_{\rm SP}^{\rm st}+V_{\rm SP}^{\rm pol}$. Due to the insulator character of the surface, both term can be derived by considering the surface as composed by independent target ions. Consequently, the static potential $V_{\rm SP}^{\rm st}$ is expressed as a sum of individual interatomic potentials $V_{\rm st}(\vec{R})$, which represent the static interaction of the incident atom with solid ions placed at different lattice sites [8]. Following the Lenz energy functional [12,13], for the two types of target ions—alkali-metal and halide—the static ion-atom interaction is found to be the sum of three terms

$$V_{\rm st}(\vec{R}) = V_{\rm Coul}(\vec{R}) + V_{\rm kin}(\vec{R}) + V_{\rm xch}(\vec{R}). \tag{8}$$

The first term is the well-known electrostatic Coulomb interaction

$$V_{\rm Coul}(\vec{R}) = \frac{1}{2}\int\int d\vec{r}d\vec{r}' D_T(\vec{r})\frac{1}{|\vec{r}-\vec{r}'|}D_P(\vec{r}'-\vec{R}), \tag{9}$$

where $D_T(\vec{r})=Z_T\delta(\vec{r})-\rho_T(\vec{r})$ and $D_P(\vec{r})=Z_P\delta(\vec{r})-\rho_P(\vec{r})$ are the target and projectile charge densities, δ is the Dirac delta

function, situated at the position of the nucleus, $Z_T(Z_P)$ is the target (projectile) nucleus charge, and $\rho_T(\rho_P)$ is the target (projectile) electronic density. Note that V_{Coul} is composed by four terms, including the internuclear and electron-electron repulsions as well as the attractive electron-nucleus potentials.

By employing the Abrahamson approximation [9] the second term of Eq. (8), called the kinetic potential, reads

$$V_{\mathrm{kin}}(\vec{R})\frac{1}{2.871} = \int d\vec{r}[\rho_T(\vec{r}) + \rho_P(\vec{r}-\vec{R})]^{5/3} - \int d\vec{r}\rho_T^{5/3}(\vec{r}) - \int d\vec{r}\rho_P^{5/3}(\mathbf{r}-\vec{R}). \tag{10}$$

This potential is essentially positive and represents the reaction to the compression of the electronic density, considered as a free-electron gas. The third term describes the exchange potential within the local approximation and it reads

$$V_{\mathrm{xch}}(\vec{R})\frac{(-1)}{0.738} = \int d\vec{r}[\rho_T(\vec{r}) + \rho_P(\vec{r}-\vec{R})]^{4/3} - \int d\vec{r}\rho_T^{4/3}(\vec{r}) - \int d\vec{r}\rho_P^{4/3}(\vec{r}-\vec{R}). \tag{11}$$

Finally, the potential $V_{\mathrm{SP}}^{\mathrm{pol}}$ takes into account the polarization of the neutral projectile in the presence of target ions, which is not included in the original Abrahamson model. Following the usual derivation of the atomic polarization potential [5], although in this case, not for only one perturbative charge but a collection of them, which represent the different target ions, the asymptotic polarization potential reads

$$V_{\mathrm{SP}}^{\mathrm{pol}}(\vec{R}) = -\frac{\alpha}{2}\sum_{i,j}\frac{Z_{Ti}^{(\infty)}}{(R_{0i}^2+R_i^2)}(\hat{R}_i\cdot\hat{R}_j)\frac{Z_{Tj}^{(\infty)}}{(R_{0j}^2+R_j^2)}, \tag{12}$$

where the sum formally includes all the target ions of the crystal, α is the polarizability of the projectile, with $\alpha = 1.38$ a.u. for helium [14] and $\vec{R}_i$ ($\vec{R}_j$) represents the position vector of the projectile with respect to the target ion labeled as i (j), with $\hat{R}_i = \vec{R}_i/R_i$. In Eq. (12), $Z_{Ti}^{(\infty)}$ is the residual charge of the target ion at long distances, being $Z_{Ti}^{(\infty)}=1$ for Li^+ and $Z_{Ti}^{(\infty)}=-1$ for F^-. At short distances the polarization contribution of the target ion i is reduced with a cutoff, which is always of the order of the radius of the atom, that is, $R_{0i} = \langle r\rangle_{Ti} + \langle r\rangle_P$, where $\langle r\rangle_{Ti}(\langle r\rangle_P)$ is the target (projectile) mean radius. We employed the values 1.09, 0.67, and 1.41 a.u. for the He, Li^+, and F^- mean radii, respectively. Far from the surface, the diagonal terms ($i=j$) of the polarization potential given by Eq. (12) satisfy the well-known behavior $-\alpha/2R^4$, but the extradiagonal terms ($i \neq j$) are weighted by a directional factor that depends on the crystal ordering [15,16]. Notice that as we are dealing with neutral projectiles, we have not taken into account the dynamic polarization of the surface ions [8] because this effect represents a higher-order correction of the interatomic potential ($\propto R^{-6}$).

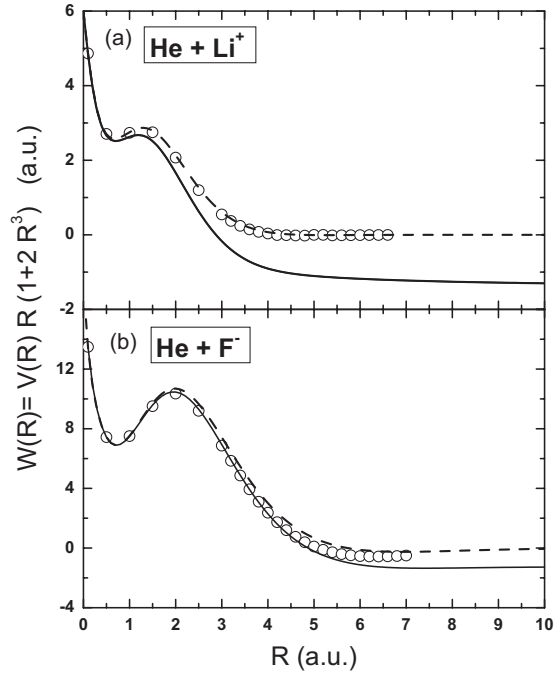

FIG. 2. Scaled interatomic potentials for (a) He-Li^+ and (b) He-F^-. Solid line, potential including the diagonal ($i=j$) polarization contribution; dashed line, static potential, without polarization; and empty circles, results reported by Gordon and Kim in Ref. [19].

IV. RESULTS

We applied the model to neutral helium atoms impinging grazingly on a LiF crystal surface under axial surface channeling conditions. The impact energy ranged from 0.2 to 8.6 keV, corresponding to the experiments of Refs. [1–3]. In the crystal surface, ions belonging to the topmost atomic layer were slightly displaced from their equilibrium positions, in accord with Ref. [17].

To describe the projectile-surface potential we employed the punctual model of Ref. [8], evaluating the He-Li^+ and He-F^- interatomic potentials from Eq. (8). Hartree-Fock Slater wave functions from Clementi-Roetti [18] were used to calculate the electronic densities ρ_T and ρ_P. It allowed us to derive a closed form for V_{Coul}, while V_{kin} and V_{xch} were obtained from numerical integrations. In Fig. 2 it seemed convenient to plot the scaled expression $W(R)=V(R)R(1+2R^3)$ for Li^+ and F^-, respectively, where $V(R)$ includes the static potential [Eq. (8)] plus the diagonal polarization contribution, i.e., the $i=j$ term of Eq. (12). From the figure we can differentiate two different regions of the interatomic potentials. As $R\to 0$, $W(R)\to Z_T Z_P$ and the sharp increase at the origin corresponds to the electrostatic contribution $V_{\mathrm{Coul}}(R)$, while the maximum at intermediate distances is mainly due to the statistical contribution, i.e., $V_{\mathrm{kin}}(R)+V_{\mathrm{xch}}(R)$. Note that present static potentials are almost indistinguishable from the ones of Gordon and Kim [19] (empty circles), employed in Ref. [3]. The asymptotic limit of V as $R\to\infty$ is affected by the polarization, i.e., $VR(1+2R^3)\to -\alpha$.

The projectile trajectory was derived from classical dynamics with the Runge-Kutta method. At every step we took into account the fourth-order nearest-neighbor target ions

(i.e., $8\times8\times4$), which includes the interaction of the projectile with the topmost atomic layer and three more layers below it. We have made sure our results do no depend on the considered number of nearest neighbors by increasing this number to include up to eighth-order nearest-neighbors (i.e., eight atomic planes).

The evaluation of the eikonal transition matrix involves an integration on the starting point $\vec{R}_{os}$ of the classical trajectory, which was calculated with the Monte Carlo technique, varying $\vec{R}_{os}$ on the area of the unit cell as a consequence of the surface invariance. In every case we considered around 10^5 classical trajectories with random initial positions, and this number was varied in order to test the convergency of our calculations. The further integration on t involved in Eq. (6) was numerically solved with a relative error lower than 0.1%. To obtain the differential probability $dP/d\Omega_f$, we have to add the T-matrix elements corresponding to different values of $\vec{R}_{\rm os}$ that lead to the same final momentum $\vec{K}_f$. For this purpose we employed a grid for the angles θ_f and φ_f of 100×100 points, where θ_f and φ_f are the final polar and azimuthal angles, respectively, of the final momentum $\vec{K}_f$. In all calculations we oriented the $\hat{x}$ versor along the low-index direction of the crystal surface coinciding with the impact direction; therefore, the azimuthal angle φ_f is measured with respect to the incidence direction on the surface plane (see Fig. 1). In full accord with the experiments of Refs. [1–3] we found that under axial surface channeling conditions the relation $\theta_f^2+\varphi_f^2\simeq\theta_i^2$ is almost strictly verified by all classically scattered projectiles and consequently, the angular projectile distribution shows the usual banana shape [20].

We start the analysis by considering the experimental case of Fig. 5 of Ref. [1]; that is, 3 keV ^{3}He atoms impinging on a LiF(001) surface along the crystallographic direction $\langle110\rangle$ with a glancing angle ($\theta_i=1.1°$). This collision system looks adequate for the eikonal description because the de Broglie wavelength of the incident atom ($\lambda=0.0057$ a.u.) is almost three orders of magnitude smaller than the characteristic interatomic distance. In Fig. 3 we plot the differential probability $dP/d\varphi_f$, as a function of the azimuthal angle φ_f, multiplying the results by an arbitrary factor in order to show the different curves separately. The eikonal spectrum displays strong interference signatures, presenting pronounced maxima symmetrically placed with respect to the incidence direction, which corresponds to $\varphi_f=0$. This interference pattern can be directly compared with the experimental spots of Ref. [1], which are displayed with stars, numbering them from the central one. The eikonal distribution nearly agrees with the experimental one, although the eikonal maxima associated to the peaks ±1, ±2, ±3, and ±4 are slightly shifted to higher values. Notice that the extreme angles of the eikonal spectrum are related to the rainbow scattering and the corresponding maxima display a sharp shape. These peaks are also present in the classical distribution, defined as the number of projectile trajectories reaching a given final azimuthal angle φ_f, which is shown in an absolute scale in Fig. 3. The classical scattering distribution presents the typical rainbow profile [21], with only two maxima around the extremes of the angular spectrum—the rainbow angles. Then, the absence of intermediate structures in the classical spectrum confirms the concept that interference effects are a consequence of quantum coherence between projectiles moving along different paths but ending in the same final state.

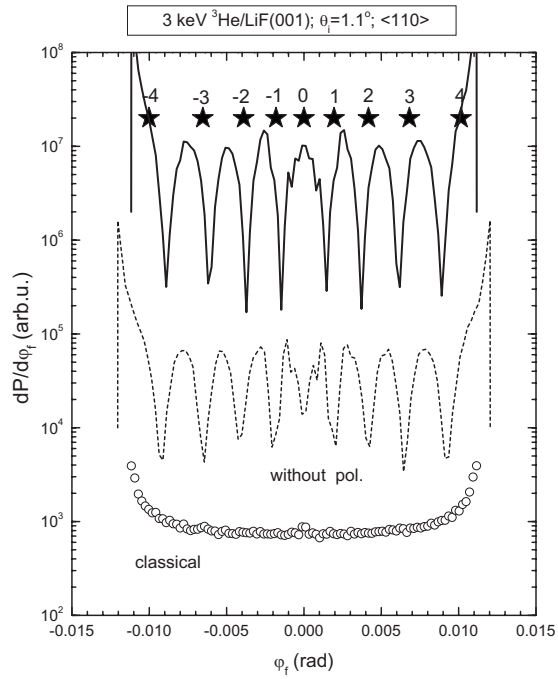

FIG. 3. Azimuthal angular distribution of elastic scattered projectiles for 3 keV ^{3}He atoms impinging on LiF(001) along the direction $\langle110\rangle$, with the incidence angle $\theta_i=1.1°$. Solid line, differential probability derived from the surface eikonal approach, including polarization effects; dashed line, surface eikonal results without including the projectile polarization. Full stars, experimental spots of Fig. 5 of Ref. [1]. Empty circles, classical distribution, as explained in the text, in absolute scale.

With the aim of analyzing the influence of the polarization of helium atoms, in Fig. 3 we also plot eikonal values obtained by neglecting the polarization potential; that is, by dropping $V_{\rm SP}^{\rm pol}$ in the projectile-surface interaction. We found that for incidence along the direction $\langle110\rangle$, the angular distribution of scattered atoms is affected by the projectile polarization. When the polarization is not included in the calculation, the central maximum becomes a minimum, modifying the total number of peaks displayed by the eikonal distribution. In turn, the extreme maxima, associated with the rainbow angles, are only slightly altered by the polarization. Both angular regions—central and external—of the eikonal spectrum are associated with different zones of the interatomic potentials that are probed by axial channeled projectiles. He^0 atoms that reach azimuthal angles φ_f near 0 move over the ionic rows that form the channel, farther than 2 a.u. from the surface, interacting with the long-distance contribution of the surface-projectile potential. As a such contribution is dominated by the term corresponding to the polarization potential, given by Eq. (12), it explains the influence of this effect on the central zone of the spectrum. Projectiles that end in the rainbow angular region, instead, suffer closer collisions with F ionic centers, being affected by the short-

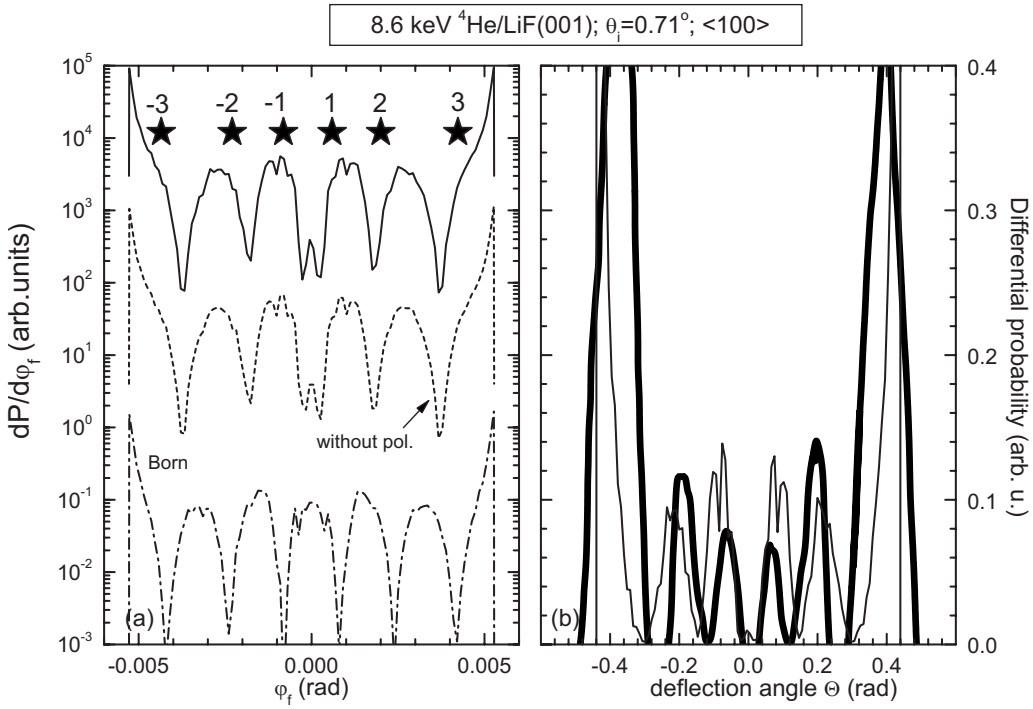

FIG. 4. Similar to Fig. 3 for 8.6 keV ^{4}He atoms impinging on LiF(001) along the direction ⟨100⟩, with the incidence angle θ_i=0.71°. Dash-dotted line, first Born approximation [Eq. (7)]. (a) Full stars, experimental spots, and (b) thick solid line, experimental intensity, both drawn from Fig. 2 of Ref. [3].

distance behavior of the interatomic potentials, which is determined by Coulombic and statistical contributions.

In Fig. 4 we investigate the elastic scattering along the direction ⟨100⟩ by considering a higher impact energy (8.6 keV). The eikonal differential probability is plotted in Fig. 4(a) as a function of the final azimuthal angle, together with experimental spots of Fig. 2 of Ref. [3]. For this collision system, in addition to the two rainbow maxima, the eikonal distribution presents four similar peaks, symmetrically placed around φ_f=0, and a very small central maximum. The number of main maxima of the eikonal profile coincides with that of the experimental pattern [3], although the positions of the peaks are again shifted to higher values in comparison with the experimental ones. In all the cases we found that slight changes in the interatomic potentials produce substantial modifications in the angular spectrum of scattered projectiles. Hence, discrepancies between theoretical and experimental spectra could be associated with very subtle differences in the projectile-surface potential. In Fig. 4(b) we compare experimental intensities [3] with eikonal probabilities, now plotted in linear scale, as function of the deflection angle Θ, defined as $\Theta=\arctan(\varphi_f/\theta_f)$. Taking into account that our theoretical results were obtained by considering fixed positions of the target ions, without including the thermal vibration, and they were not convoluted with experimental conditions, the eikonal model reproduces fairly well the main features of the experimental spectrum.

In order to investigate the effect of the polarization in the channel ⟨100⟩, in Fig. 4(a) we show eikonal values derived by eliminating the polarization potential. Remarkably, eikonal results with and without including the projectile polarization agree with each other for incidence along the ⟨100⟩ direction, indicating that polarization effects play a minor role in this channel. It is a consequence of the ordering of the halide and alkali ions involved in the axial surface channeling. As observed from Eq. (12), when the projectile moves along the channel far from the surface plane, the factors of the polarization potential coming from F^- and Li^+ have opposite signs and they compensate their contributions to order r^{-4} when F^- and Li^+ ions are placed in front of each other, as it happens in the ⟨100⟩ direction. Furthermore, within a row model, the ⟨100⟩ rows—formed by alternate cations an anions—display a neutral charge, which reduces the polarization of the incident atom. In the ⟨110⟩ direction, instead, not only are there separated cation and anion rows, with positive and negative net charges, respectively, but also Li^+ and F^- ions are not in front of each other along the channel, which originates an effective polarization potential. This is the reason why polarization effects become evident for incidence along the ⟨110⟩ direction but not in the channel ⟨100⟩.

In addition, in Fig. 4(a) we also show the angular distribution obtained within the first Born approximation [Eq. (7)], which is derived from Eq. (6) by eliminating the eikonal phase. The Born profile displays a different diffraction pattern, with a broad central maximum, not present in the experiment, indicating that interference structures of the surface eikonal model are affected by the phase η, given in Eq. (5). However, note that differences between eikonal and Born distributions vary with the considered collision system.

Finally, in Fig. 5 we considered the incidence conditions of Ref. [2], which correspond to a smaller impact energy (0.2 keV). Notice that this energy is close to the limit of validity of the eikonal model, which is expected to be adequate for high velocities. For scattering along the direction

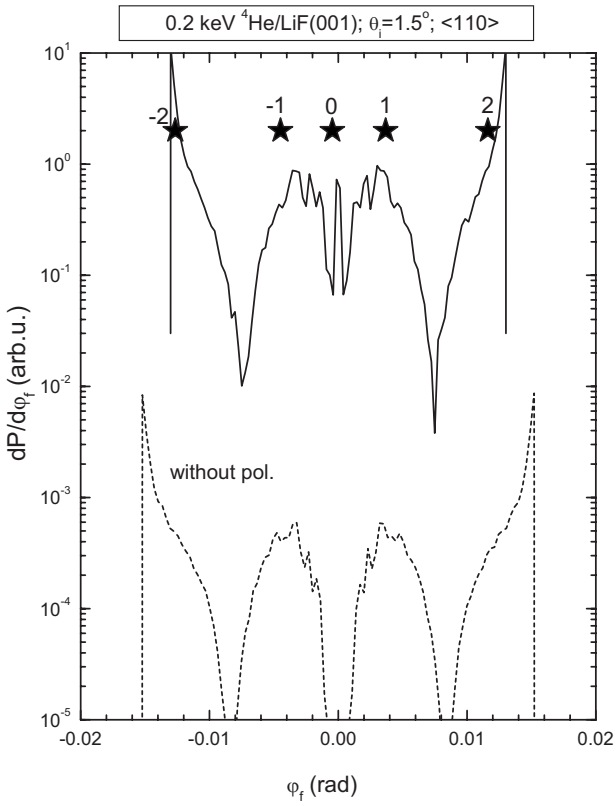

FIG. 5. Similar to Fig. 3 for 0.2 keV ^{4}He atoms impinging on LiF(001) along the direction ⟨110⟩, with the incidence angle $\theta_i = 1.5°$. Full stars, experimental data from Fig. 1 of Ref. [2].

⟨110⟩, the eikonal differential probability is displayed in Fig. 5, as a function of the azimuthal angle, comparing it with the spots of Fig. 1 of Ref. [2]. Also in this case, the agreement of the eikonal theory with the experiment is reasonable good. Both profiles—eikonal and experimental—present similar structures, with a central maximum and two additional peaks, not equally spaced, to each side. However, the experimental peaks ± 1 are narrower than the eikonal ones, and small structures around the rainbow angles are absent in the theory, corresponding to the worst disagreement found in the present work. Discrepancies between the theory and the experiment can be again attributed to extremely subtle distinctions in the projectile-surface potential. Moreover, we should mention that the small rumpling ($d = 0.037$ a.u.) of the surface ions introduced in our model [17] affects the interference pattern.

Again, as in Fig. 3, the central zone of the eikonal spectrum of Fig. 5 is associated with the long-distance behavior of the surface interaction, which is governed by the projectile polarization. When V_{SP}^{pol} is dropped, the central maximum of the eikonal distribution completely disappears, in disagreement with the experimental data.

To investigate in detail the central zone of the eikonal spectrum, in Fig. 6 we plot the first ten projectile trajectories, provided by the Monte Carlo code, that contribute to the distribution at the final azimuthal angle $\varphi_f \cong 0$. For the collision system of Fig. 3 we observe that all the atoms that end in this angular region move just over F^- or Li^+ rows. In this case, turning points corresponding to the z movement are almost independent of the motion perpendicular to the scattering plane, being approximately situated 2.8 a.u. (2.2 a.u.)

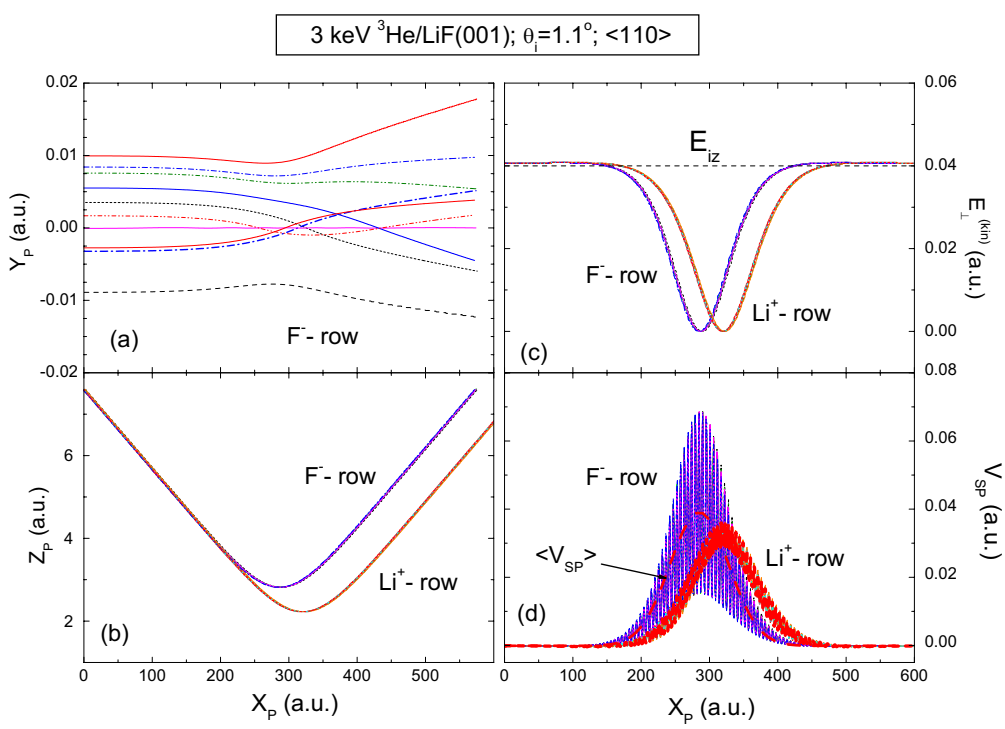

FIG. 6. (Color online) Classical projectile trajectories ending with a final azimuthal angle φ_f near to 0, as a function of the coordinatate X_P parallel to the axial channel, for the collision system of Fig. 3. (a) Coordinate Y_P perpendicular to the scattering plane; (b) coordinate Z_P perpendicular to the surface; (c) transversal kinetic energy along the trajectory, defined as $E_\perp = m_P(v_y^2 + v_z^2)/2$; (d) projectile-surface potential along the trajectory.

above the topmost atomic layer for projectiles moving over F^- (Li^+) rows. From Fig. 6(c), the transversal kinetic energy, defined as $E_\perp^{\rm kin}=m_P(v_y^2+v_z^2)/2$, slightly increases just before and after reaching the collision region, indicating that incident atoms are affected by an attractive polarization potential. The projectile-surface potential along classical trajectories, shown in Fig. 6(d), displays an oscillatory pattern produced by the interaction with the different ionic centers of the crystal surface. Consequently, the total transversal energy $E_\perp=E_\perp^{\rm kin}+V_{\rm SP}$ presents fluctuations along the classical projectile path. However, the mean value $\langle E_\perp\rangle=\langle E_\perp^{\rm kin}\rangle+\langle V_{\rm SP}\rangle$ keeps equal to the initial value $E_{iz}=m_P v_{iz}^2/2$ along the whole trajectory, supporting to some extend the decoupling of the transversal movement from the parallel one, proposed in Ref. [2].

V. SUMMARY

In conclusion, we have developed a surface eikonal approach to deal with interference patterns produced by impact of swift atoms on insulator surfaces. The proposed method has been applied to few-keV He atoms grazing impinging on LiF(001) along the ⟨110⟩ and ⟨100⟩ directions. Projectile spectra derived with the eikonal approximation display well-defined interference structures, originated by atoms that follow different paths but end scattered with the same final momentum. As the projectile distribution strongly depends on the description employed to represent the projectile-surface interaction, the study focused on the influence of the projectile polarization on the angular spectrum. We conclude that the polarization potential is essential to describe the elastic scattering along the ⟨110⟩ channel, while in the direction ⟨100⟩ its contribution is negligible. Angular spectra derived from the eikonal model, including the polarization effect, are in concordance with the available experimental data [1–3]. But a better representation of the surface potential, taking into account that target ions are part of a surface, might modify the present results. Then, by including more precise electronic densities this method may be useful to investigate very delicate items, such as long-distance potentials or crystal ion displacements, which are difficult to make evident experimentally [22].

ACKNOWLEDGMENTS

This work was supported by CONICET, UBA, and ANPCyT of Argentina.

[1] A. Schüller, S. Wethekam, and H. Winter, Phys. Rev. Lett. **98**, 016103 (2007).
[2] P. Rousseau, H. Khemliche, A. G. Borisov, and P. Roncin, Phys. Rev. Lett. **98**, 016104 (2007).
[3] A. Schüller and H. Winter, Phys. Rev. Lett. **100**, 097602 (2008).
[4] W. F. Avrin and R. P. Merrill, Surf. Sci. **311**, 269 (1994).
[5] C. J. Joachain, *Quantum Collision Theory* (North-Holland, Amsterdam, 1979).
[6] R. J. Glauber, *Lectures in Theoretical Physics* (Interscience, New York, 1959), Vol. 1, p. 315.
[7] J. R. Manson and K.-H. Rieder, Phys. Rev. B **62**, 13 142 (2000).
[8] A. J. García and J. E. Miraglia, Phys. Rev. A **74**, 012902 (2006).
[9] A. A. Abrahmson, Phys. Rev. **133**, A990 (1964).
[10] M. R. C. McDowell and J. P. Coleman, *Introduction to the Theory of Ion-Atom Collisions* (North-Holland, Amsterdam, 1970).
[11] L. M. Hubbard and W. H. Miller, J. Chem. Phys. **78**, 1801 (1983).
[12] W. Lenz, Z. Phys. **77**, 713 (1932).
[13] H. Jensen, Z. Phys. **77**, 722 (1932).
[14] T. M. Miller and B. Bederson, *Advances in Atomic and Molecular Physics*, edited by D. R. Bates and B. Bederson (Academic, New York, 1977), Vol. 13, pp. 1–55.
[15] In the limit of an ideal Coulomb crystal surface, $V_{\rm SP}^{\rm pol}$ tends to Eq. (3.13) of Ref. [16] far from the surface.
[16] V. Celli, D. Eichenauer, A. Kaufhold, and J. P. Toennies, J. Chem. Phys. **83**, 2504 (1985).
[17] J. Vogt and H. Weiss, Surf. Sci. **501**, 203 (2002).
[18] E. Clementi and C. Roetti, At. Data Nucl. Data Tables **14**, 177 (1974).
[19] R. G. Gordon and Y. S. Kim, J. Chem. Phys. **56**, 3122 (1972).
[20] F. W. Meyer, L. Folkerts, and S. Schippers, Nucl. Instrum. Methods Phys. Res. B **100**, 366 (1995).
[21] A. Schüller, G. Adamov, S. Wethekam, K. Maass, A. Mertens, and H. Winter, Phys. Rev. A **69**, 050901(R) (2004).
[22] D. Farías, C. Díaz, P. Rivière, H. F. Busnengo, P. Nieto, M. F. Somers, G. J. Kroes, A. Salin, and F. Martín, Phys. Rev. Lett. **93**, 246104 (2004).